접착 및 계면 제16권 제3호, 2015년
〈연구논문(Original Article)〉
Journal of Adhesion and Interface Vol.16, No.3, 2015
http://dx.doi.org/10.17702/jai.2015.16.3.108

3-히드록시부티레이트-3-히드록시발러레이트 공중합체/그래핀 나노복합체의 제조 및 물성

유은정 · 이단비 · 하창식†

부산대학교 고분자공학과
(2015년 7월 22일 접수, 2015년 8월 27일 수정, 2015년 9월 2일 채택)

Preparation and Characterization of Poly(3-hydroxybutyrate-co-3-hydroxyvalerate)/Graphene Nanocomposites

Eun Jung You, Dan Bi Lee, and Chang-Sik Ha†

Department of Polymer Science and Engineering, Pusan National University, Busan 46241, Republic of Korea
(Received July 22, 2015; Revised August 27, 2015; Accepted September 2, 2015)

요 약: 본 연구는 poly(3-hydroxybutyrate-co-3-hydroxyvalerate) (PHBV)/그래핀 복합체의 제조 및 특성에 관한 연구이다. 투입하는 그래핀의 함량에 따른 복합체의 전기적 물성, 소수성, 및 열적 성질에 미치는 영향에 대해 연구하였다. 표면주사전자현미경 연구결과 PHBV 고분자 matrix에 판상의 그래핀이 고르게 잘 분산되었음을 확인하였다. X-선 회절 연구와 시차열량주사계 분석을 통하여 그래핀을 첨가할수록 PHBV의 결정도를 증가시켰고, 투입하는 그래핀의 함량이 증가할수록 복합체의 열적 안정성, 소수성 및 전기전도도 등이 증가하는 것으로 나타났다.

Abstract: In the present work, we investigated poly(3-hydroxybutyrate-co-3-hydroxyvalerate) (PHBV)/graphene nanocomposites. The electrical, hydrophobic properties and thermal properties of the nanocomposite films having different graphene contents were investigated. The scanning electron microscopy (SEM) morphology showed good dispersion of graphene layers in the PHBV matrix. Based on the X-ray diffraction and differential scanning calorimetry, the addition of graphene increased the crystallinity of PHBV. Thermal stability, hydrophobicity, and electrical conductivity of the nanocomposites were increased with increasing the graphene contents.

Keywords: *Poly(3-hydroxybutyrate-co-3-hydroxyvalerate), graphene, nanocomposite, electrical conductivity, hydrophobicity*

1. Introduction

There is considerable interest in polyhydroxyalkanoates (PHAs) obtained in high yield as energy storage materials from certain bacteria grown under nutrient-limited conditions. These bacteria can produce a wide range of PHAs depending on the nutrient medium on which they are grown. Polyhydroxybutyrate (PHB) and poly(3-hydroxybutyrate-co-3-valerate) (PHBV) have drawn the most commercial attention to date. Development of PHBV has been driven by the need for improvements in the mechanical properties and processability of PHB. PHBV is considered an interesting material for use in packaging because of its barrier properties[1-3] and also its compostability[4]. Cava et al. compared the properties of poly(ethylene terephthalte (PET) with those of biodegradable polymers such as polylactic acid (PLA), poly(e-caprolactone) (PCL) and PHBV and their nanocomposites. Their research showed that PHBV could withstand thermal retorting so that it is as good as those of PET.

Graphene, flat carbon nanosheets, as a single layer of carbon atoms arranged in a two dimensional honeycomb lattice, has attracted great interest because of its unique physical, chemical, electrical and mechanical proper-

†Corresponding author: Chang-Sik Ha (csha@pnu.edu)

ties[5,6], since its discovery by Novoselov et al. in 2004[7]. They have received more and more attention as a viable filler in composite materials because they could offer the high thermal and chemical stability and improved electrical conductivity[8,9].

To improve key properties of PHBV and to make it more suitable for applications in the packaging market, nanocomposites incorporating PHBV and graphene have been developed. The thermal and mechanical properties of the nanocomposite films can be increased to a large extent by adding graphene because of the effect of reinforcement in the polymer matrix. In this sense, to our knowledge, three papers have been reported on the PHBV/graphene nanocomposites till now[10-12]. They reported some interesting results on the effects of graphene on the properties of PHBV when the contents of graphene were from 2 wt% to 6 wt%. They investigated crystallization behavior, thermal and mechanical properties of the nanocomposites. In this study, however, we investigate PHBV/graphene nanocomposites in more systematic way over different composition ranges of graphene from 0.7 wt% to 5 wt% with their further hydrophobicity and electrical conductivity behavior, which were not investigated in those previous works.

2. Experimental

2.1. Materials

Natural graphite powder (< 20 μm), potassium persulfate, phosphorus pentoxide, photassium permanganate, hydrogen peroxide solution (30 wt%), hydrochloric acid (37%) and poly(3-hydroxybutyrate-co-3-hydroxyvalerate), otherwise known as PHBV, containing 12 mol% of valerate (PHBV) were purchased from Sigma Aldrich and used after oven drying at 60°C for 24 h. Sulfuric acid (97%) was purchased from Junsei.

Graphene oxide (GO) was synthesized from graphite powder by the modified Hummers method[13]. Briefly, graphite powders (1.0 g), $K_2S_2O_8$ (0.50 g) and P_2O_5 (0.50 g) were added to 3.0 mL of conc. H_2SO_4 with stirring until the reactants are completely dissolved.

The mixture is kept at 80°C for 4.5 h, after which heating was stopped and the mixture is diluted with 1.0 L of Millipore water. The mixture was filtered and washed to remove all traces of acid. For the oxidation step of the synthesis, the pretreated graphite is added to 26 mL of H_2SO_4 with stirring. To this reaction mixture, 3.0 g of $KMnO_4$ was added slowly in an ice bath to ensure that the temperature remained below 10°C. Then, this mixture reacts at 35°C for 2 h after which 46 mL of distilled water is added in an ice bath. This mixture is stirred for 2 h at 35°C, after which heating is stopped and the mixture is diluted with 140 mL of water and 2.5 mL of 30% H_2O_2 is added to the mixture. After the resulting mixture turns yellow, the mixture is allowed to settle for at least a day after which the clear supernatant is decanted. The remaining mixture is filtered and washed with a 1.0 L of 10% HCl solution. The resulting solid is dried in air and diluted in distilled water that is put through dialysis for 2 weeks to remove any remaining materials and residues, after which the product was centrifuged and washed several times with Millipore water to neutralization and remove residual species. Finally, the dark brown GO powders were obtained through drying at 50°C in a vacuum oven for a day. The GO powder dissolved in a known volume of water was subjected to ultrasonication for 40 min to give a stable suspension of GO (typically conc. 0.50 mg/mL) and then centrifuged at 4000 rpm for 10 min to remove any aggregates remained in the suspension. To reduce individual GO platelets into graphene, thermal shock of GO powders at temperatures up to ~1100°C has been used[14].

For the preparation of composites, graphene was dispersed in chloroform with stirring for 12 h, followed by ultrasonication for 30 min. PHBV was dissolved in chloroform at 60°C with stirring for 2 h. In order to examine the effect of graphene content on the properties of the composite materials, we formulated graphene contents of 0, 0.7, 1, 2 and 5 wt% with respect to the PHBV content. Solution of graphene was poured into the solution of PHBV and stirring was continued for 2 h. Then, the mixture was sonicated for 30 min to make a well dispersed suspension. A good dispersion of graphene in the polymer matrix is required because the properties of the composites are determined by the dispersion of graphene. Finally, samples were dried in a vacuum oven at 35°C to constant weight. The film was peeled off from a substrate for further testing. A series of PHBV / graphene nanocomposites with various graphene loadings were similarly prepared.

2.2. Characterization

Wide-angle X-ray diffraction (WAXD) measurements were performed using a conventional x-ray diffractometer

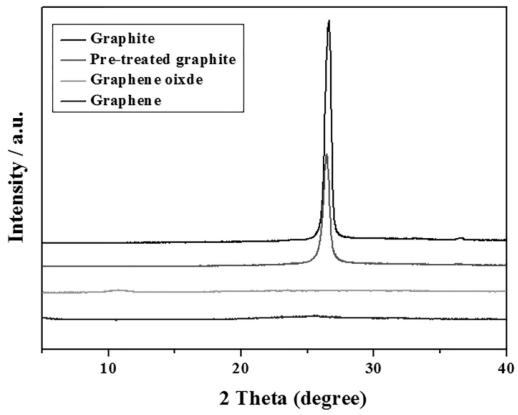

Figure 1. XRD patterns of graphite, preoxidated graphite, graphene oxide and graphene.

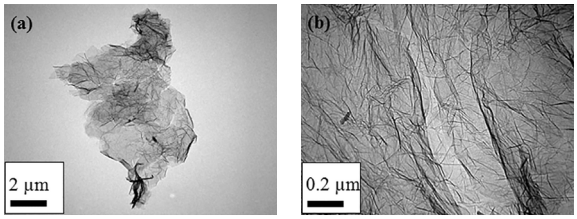

Figure 2. TEM images of graphene with (a) low and (b) high magnification.

[Rigaku Miniflex, CuKα (λ = 1.5418 Å)] at a scan speed of 1 °/min. Raman spectra were recorded from 1000 to 2000 cm^{-1} using a FT-Raman spectrometer (FRS-100S, Bruker) with an argon ion laser using an excitation wavelength of 514.5 nm. Thermogravimetric analysis (TGA) was performed using a thermogravimetric analyger (TGA) (Q500 Series, TA Instrument). The heating rate was 10 °C/min over the temperature range, 30 and 800°C, under a nitrogen atmosphere. A differential scanning calorimetry (DSC) analysis was carried out on Q 100 (N_2 flow). Each sample was heated from 30 to 300°C at a heating rate of 20°C /min. The Fourier transform Infrared (FT-IR) spectra of the films were measured using a spectrometer (react IRTM 1000, Applied System, ASi). The surface resistance and electrical conductivities of the PHBV/graphene nanocomposite films were measured using surface resistance tester (ST-3, SIMCO). Water contact angles were measured by Krüss Drop Shape Analysis system.

3. Results and Discussion

Figure 1 shows the XRD patterns of natural graphite, pre-oxidated graphite, graphene oxide and graphene. The

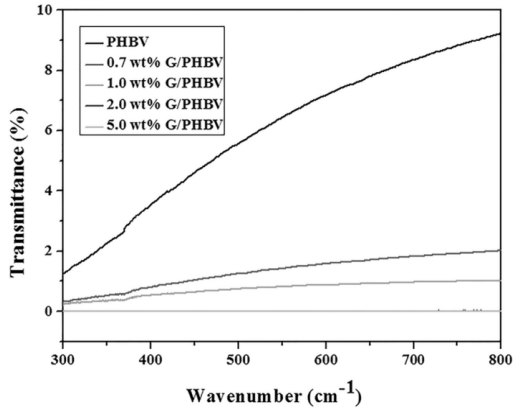

Figure 3. UV-vis spectra of PHBV/graphene nanocomposites with different graphene weight percentages.

characteristic peaks of graphite, pre-oxidated graphite and graphene oxide appear at 2θ = 26.62, 26.48° and 10.53°, respectively. Graphene showed no peaks because of the full exfoliation of GO sheets. From the Bragg equation ($2d\sin\theta = n\lambda$) the interlayer distance of graphite, pre-oxidated graphite and graphene oxide are estimated at 3.34, 3.36 Å and 8.39 Å, respectively. These results clearly explained that the GO sheets are well exfoliated into the graphene single sheets.

Figure 2 shows the TEM images of graphene. Graphene exhibits typical wrinkled structure with corrugation and scrolling which is intrinsic to graphene. graphene used in this work might contain one- to a few-layer sheets.

UV-vis spectra were used to confirm the dispersion of graphene in the PHBV matrix. Figure 3 shows the UV spectra of the PHBV/graphene nanocomposite films with various graphene contents (0, 0.7, 1, 2, 5 wt%). It can be seen that pristine polymer showed some transparency below 10% in the wavelength range from 400 to 800 nm. Because of the well dispersion of graphene throughout the polymer matrix, the films were homogeneously dark brown. This indicates that the graphene sheets in the PHBV matrix were well dispersed on the nano scale.

Figure 4 shows the FT-IR spectra of PHBV and the PHBV/graphene nanocomposite films, with the stretching vibrations of hydroxyl (O-H) and carbonyl (C=O) groups. All the characteristic absorption peaks of PHBV appear in PHBV/graphene nanocomposites. The hydrazine hydrate treatment eliminated all of GO bands, giving evidence for the almost removal of the oxygen-containing groups, which is nearly similar with graphite spectrum. For pure PHBV, it shows its own characteristic absorp-

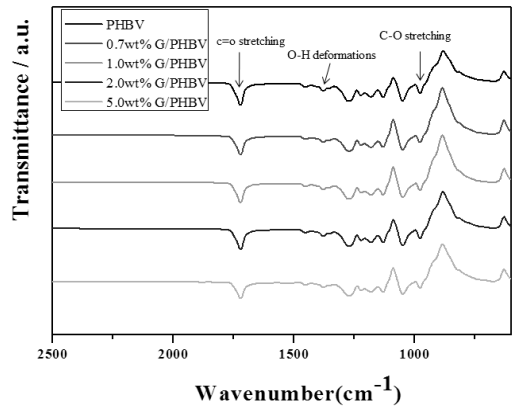

Figure 4. FT-IR spectra of PHBV/graphene nanocomposites with different graphene weight percentages.

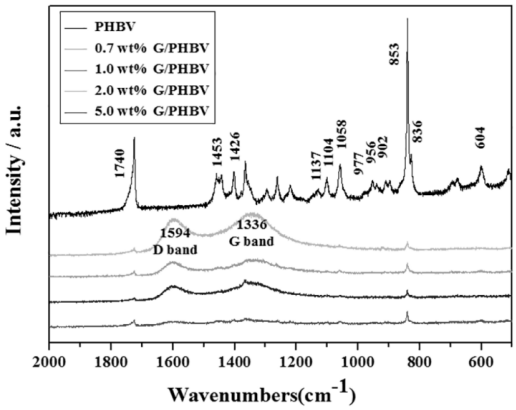

Figure 5. Raman spectra of PHBV/graphene nanocomposites containing 0 wt%, 0.7 wt%, 1.0 wt%, 2.0 wt% and 5.0 wt% of graphene.

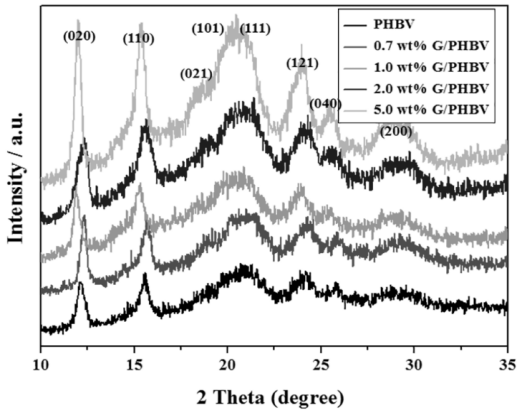

Figure 6. XRD patterns of PHBV/graphene nanocomposites with different graphene weight percentages.

tion band from 800 cm^{-1} to 975 cm^{-1}, corresponding to symmetric -C-O-C- stretching vibration. On the other hand, the antisymmetric -C-O-C-stretching leads to bands between 1060 cm^{-1} and 1150 cm^{-1}. The absorption band at 1725 cm^{-1} is due to the C=O stretching in PHBV[15].

Raman spectroscopy is a widely used tool for the characterization of carbon products, especially considering the fact that conjugated and carbon-carbon double bonds lead to high Raman intensities. Therefore, Raman spectroscopy has been used to probe structural and electronic characteristics of graphite materials, providing useful information on the defects (D band) and in-plane vibration of sp^2 carbon atoms (G band). Figure 5 shows the Raman spectra of PHBV and PHBV/graphene nanocomposites. The Raman spectrum of graphene exhibits a higher relative D/G intensity ratio (1.17) compared to GO (0.83), implying the decreased size of the sp^2 domains upon localized chemical reduction of the GO by hydrazine[12]. This high D/G intensity of graphene suggests some possibilities of exfoliation of graphene single nano sheets from graphite oxide layered structure, and it is consistent with XRD diffraction patterns. In addition, with increase in the graphene concentration, the intensity of G band and D band gradually increased.

Figure 6 shows XRD patterns of pristine PHBV and its nanocomposites with graphene. The WAXD diffractograms of recast PHBV and PHBV/graphene nanocomposites show a semicrystalline nature with its characteristic reflections corresponding to an orthorhombic cell oh PHBV[16]. Both PHBV and PHBV/graphene show reflections at the same values as for the neat biopolymer, indicating that addition of graphene does not alter the unit cell after incorporation of graphene. A comparison of the spectrum of pure PHBV with that of the PHBV/graphene nanocomposites shows that the d-spacing values are constant for all crystallographic planes, which indicates that the PHBV unit cell is not changed after becoming incorporated with graphene. As has been discussed in the literature[17], the crystal structure of the polymer was not affected by the addition of graphene. However, by the addition of graphene, the diffractogram presents a better resolution for peaks (020), (110), (121), and (200) than that of PHBV. Furthermore, the intensities of the crystalline peaks of the nanocomposite obviously increased, especially for I (200). These results confirm that the crystallization of PHBV is promoted by the addition of graphene, which is in agreement with the DSC data (Figure 7). It should be pointed out that crystallite growth of PHBV varies in different directions. There is a sharp rise of I (200) in PHBV crystals in the PHBV/graphene nanocomposites,

Table 1. Thermal Data of the PHBV/graphene Nanocomposites

Graphene Content (wt%)	T^1_d (°C)[a]	T^5_d (°C)[b]	T^{10}_d (°C)[c]	Tg (°C)[d]	Tm (°C)[e]
0	161	207	247	8.4	146
0.7	168	209	251	8.6	147
1.0	165	217	254	9.0	146
2.0	174	220	255	10.7	148
5.0	199	264	270	11.0	152

[a] Thermal degradation temperature of 1 wt% loss by TGA
[b] Thermal degradation temperature of 5 wt% loss by TGA
[c] Thermal degradation temperature of 10wt% loss by TGA
[d] Tg determined by DSC
[e] Tm determined by DSC

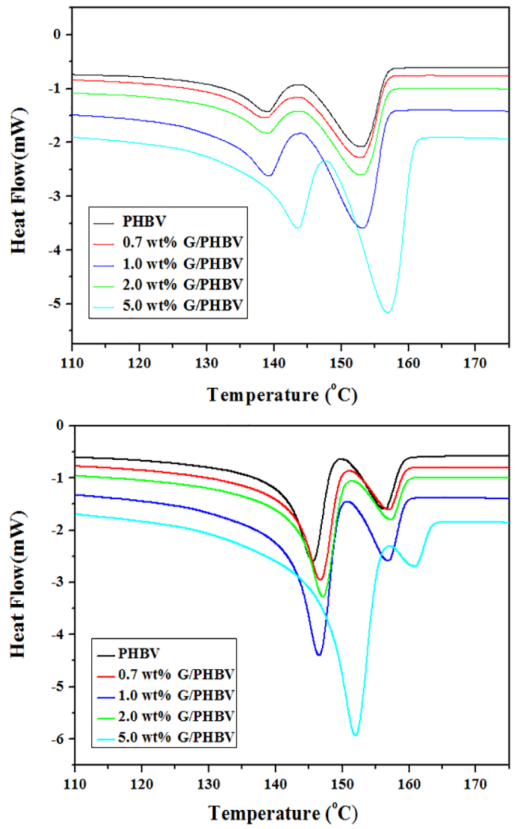

Figure 7. (a) Melting transition scans (first melting behavior) and (b) melting transition scans (second melting behavior) of PHBV/graphene nanocomposites with different graphene weight percentages at 10°C/min by DSC.

which indicated that the crystallite growth of PHBV along the direction of the *a* axis was more sensitive and preferential than that along other directions[18].

DSC was used to measure the glass transition temperatures of the pure PHBV and PHBV/graphene nanocomposites. Figure 7 shows the DSC data for neat PHBV and its graphene nanocomposites. A bimodal endothermic melting peak in the heating mode is observed in all the samples corresponding to the formation of two crystalline phases with different sizes of lamellae of varying thickness. With increase in the graphene concentration, there was a progressive increase in melting peak temperatures (see Table 1). This can be explained on the basis of hetero and homogeneous nucleation of PHBV. It has been reported that the two melting peaks of PHBV correspond to the heterogeneous nucleation of PHBV occurring due to chain aggregation and the higher temperature peak is related to homogeneous nucleation. Our result indicates that the addition of graphene influences both types of nucleation[19].

The changes in the surface morphology were observed using a SEM. Figure 7 (a)-(e) shows the morphology of nanocomposites containing graphene nanosheets with various graphene contents. SEM measurements provide direct information regarding the interfacial interactions of these nanocomposite films. For a pure PHBV, a smooth surface was observed in the surface (Figure 7(a)). The surface of the nanocomposite films exhibits high homogeneity and smooth morphology. It clearly reveals a layered structure with uniformly dispersed graphene sheets in PHBV matrix. It means that the well-mixing behaviour of PHBV and graphene in the nanocomposite. A number of wrinkled graphene sheets were pulled out of the film. Moreover, the obvious thickness increases of these sheets compared with 1 nm-thick single graphene sheets suggested that the surfaces of graphene sheets were coated with the polymer, indicating that there were strong interfacial interactions between PHBV and graphene components.

Table 2. Electrical Properties of PHBV/graphene Nanocomposites with Different Graphene Weight Percentages

Graphene Content (wt%)	Rs (Ω/m^2)	P (Ω · m)	Conductivity (S/m)
0	-	-	-
0.7	12.5	12.5×10^{-6}	80.1×10^{3}
1.0	9.6	9.65×10^{-6}	10.4×10^{4}
2.0	8.3	8.35×10^{-6}	12.1×10^{4}
5.0	7.2	7.25×10^{-6}	13.9×10^{4}

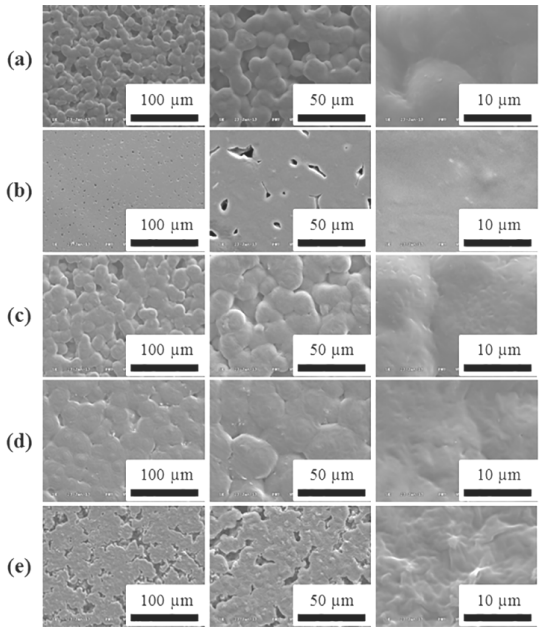

Figure 8. SEM images of PHBV/graphene nanocomposites containing (a) 0 wt%, (b) 0.7 wt%, (c) 1.0 wt%, (d) 2.0 wt% and (e) 5 wt% of graphene.

TGA experiment was carried out as a means for evaluation of thermal stability of the polymer and nanocomposites. TGA curves are shown in Figure 8. Inorganic fillers have been reported to improve the thermal stability of polymer composites, relative to the host polymer. Figure 8 shows TGA curves of the PHBV and PHBV/graphene nanocomposites. The pure PHBV polymer started to lose weight at 161°C. The presence of graphene sheets noticeably improves the thermal stability of the PHBV; the onset degradation temperature is shifted toward higher temperatures with increasing the graphene filler contents up to 199°C at PHBV/graphene (5 wt%). Since the thermal degradation of a polymer begins with chain cleavage and radical formation, the carbon surface of graphene nanofillers in the nanocomposite might act as a radical scavenger to delay the onset of thermal degradation and, hence, improve the thermal stability of PHBV[20].

The initial, 5 and 10 wt% loss temperatures on the TGA curves for the nanocomposites with different graphene loadings under nitrogen environments are summarized in Table 1. The onset temperature for degradation is 161°C for neat PHBV. The onset temperature for degradation of the nanocomposite containing 5 wt% graphene is 38°C higher than that of pristine polymer. It indicates that the thermal stability of the nanocomposites could improve with just 0.7 wt% of graphene filler. Thermal degradation temperature of 5 wt% loss is 264°C for the nanocomposite with 5 wt% of graphene addition and is 57°C higher than that of the pristine polymer. Thermal degradation temperature of 10 wt% loss of the pure PHBV is 207°C, which is 23°C higher than that of pristine polymer. It is due to the high thermal stability of graphene nanosheets in the polymer matrix.

The surface resistance values and electrical conductivities for PHBV/graphene nanocomposites are shown in Table 2. Also when increasing the graphene contents in nanocomposites, surface resistance was decreased. Pristine polymer show out of spec result, though for PHBV/graphene nanocomposites of 0.7, 1.0, 2.0 wt% and 5.0 wt% were 12.5, 9.6, 8.3 Ω/m^2 and 7.2 Ω/m^2, respectively. It means these composites can be applied for electrical materials. The conductivity of pristine polymer shows out of spec result, though for PHBV/graphene nanocomposites of 0.7, 1.0, 2.0 wt% and 5.0 wt% were 80.1×10^{3}, 10.4×10^{4}, 12.1×10^{4} S/m and 13.9×10^{4} S/m, respectively. Considering the chemical structure and morphology of the nanocomposites, its electrical properties can be well understood. Due to the electrical properties originated from the graphene and the sufficient volume of graphene, the conductivity was of the order of 13.9×10^{4} S/m at 5 wt% of graphene. When the conductive network became perfectly established, the conductivity of the PHBV/graphene nanocomposites will be increased. A previous work demonstrated that the electri-

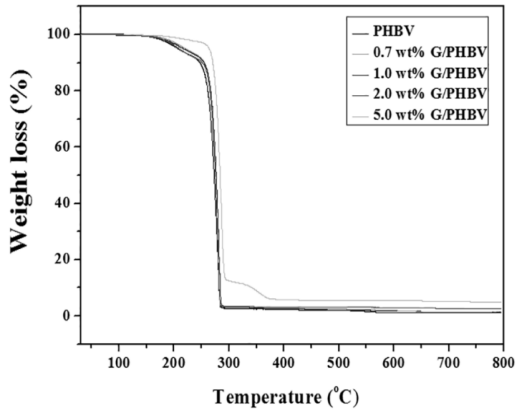

Figure 9. TG Analysis of PHBV/graphene nanocomposites with different graphene weight percentages.

cal conductivity of the PET/Graphene nanocomposite increased from 2.0×10^{-13} to 7.4×10^{-2} S/m[21].

As shown in Figure 10, the water contact angle for pure PHBV was 86.7 ± 1.0°, while for PHBV/graphene nanocomposites of 0.7, 1.0, 2.0 wt% and 5 wt% were 91.6 ± 0.6, 93.6 ± 1.8, 103.7 ± 1.1° and 111.6 ± 0.6°, respectively. This indicated that the water contact angle of graphene based PHBV nanocomposites increased with the increase in the ratio of graphene contents. That is to say, the present graphene based PHBV nanocomposites showed improved surface de-wetting properties with the increase in the ratio of graphene content in composites. This phenomenon is due to the hydrophobic property of graphene sheets.

4. Conclusions

In conclusion, we have presented a nanocomposite consisted of uniformly dispersed graphene in PHBV matrix and successfully prepared with various graphene contents by solution blending method. SEM morphology showed good dispersion of graphene layers in the PHBV matrix. XRD and DSC studies showed increase in crystallinity accompanied with increase in crystallite size due to addition of graphene. Thermal stability of the composites were improved with increase the graphene contents. The degradation temperature determined through TG analysis increased from 161°C for the pure PHBV up to 199°C for 5 wt% of PHBV/graphene nanocomposite. Water contact angle for PHBV/graphene nanocomposites also increased from 86.7 ± 1.0° to 111.6 ± 0.6°. It means the surface de-wetting property is improved with

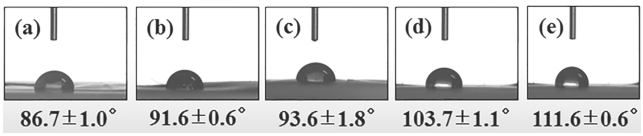

Figure 10. Contact angle images of water for (a) PHBV and PHBV/graphene nanocomposite films of (b) 0.7, (c) 1.0, (d) 2.0 and (e) 5.0 wt%.

increase graphene contents due to the hydrophobicity of the graphene sheets. We also checked the surface resistance values to investigate the electrical properties of prepared composites. Composite with 5 wt% of PHBV/graphene showed very low surface resistance value, 7.2 Ω/m^2 and high conductivity value, 13.9×10^4 S/m. The PHBV/graphene nanocmposites with high contents of graphene showed improved thermal, de-wetting, electrical properties compared to pristine PHBV polymer. The PHBV/graphene nanocmposites may have potential applications in packaging films as well as electronic devices.

Acknowledgments

The work was supported by the Ministry of Science, ICT & Future Planning, Korea (NRF-Russia Foundation for Basic Research (RFBR) Joint Research Program (No. 2013K2A1A707627); Pioneer Research Center Program (No. 2010-0019308/2010-0019482); Acceleration Research Program (2014R1A2A1110054584); Brain Korea 21 Plus Program (21A2013800002)).

Reference

1. R. Shogren, *J. Environ. Polym. Degr.*, **5**, 91 (1997).
2. D. Cava, A. López-Rubio, L. Cabedo, E. Giménez, J. L. Feijoo, R. Gavara, and J. M. Lagarón, In: Proceedings of the 63rd Annual Technical Conference & Exhibition Society of Plastics Engineers; Brookfield, CT. (2005).
3. D. Cava, E. Gimenez, R. Gavara, and J. M. Lagaron, *J. Plast. Film Sheet*, **22**, 265 (2006).
4. S. Wang, C. Song, G. Chen, T. Guo, J. Liu, B. Zhang, and S. Takeuchi, *Polym. Deg. Stab.*, **87**, 69 (2005).
5. A. K. Geim, *Science*, **324**, 1530 (2009).
6. W. Choi, I. Lahiri, R. Seelaboyina, and Y. S. Kang, *Crit. Rev. Solid State*, **35**, 52 (2010).
7. K. S. Novoselov, A. K. Geim, S. V. Morozov, D.

Jiang, Y. Zhang, S. V. Dubonos, I. V. Grigorieva, and A. A. Firsov, *Science*, **306**, 666 (2004).
8. S. Stankovich, D. A. Dikin, G. H. B. Dommett, K. M. Kohlhaas, E. J. Zimney, E. A. Stach, R. D. Piner, S. T. Nguyen, and R. S. Ruoff, *Nature*, **442**, 282 (2006).
9. J. Lee, J. Hong, and S. E. Shim, *Macromol. Res.*, **17**, 931 (2009).
10. B. Wang, Y. Zhang, J. Zhang, Q. Gou, Z. Wang, P. Chen, and Q. Gu, *Chinese J. Polym. Sci.*, **31**, 4, 670 (2013).
11. X. Jing and Z. Qui, *J. Nanosci. Nanotechnol.*, **12**, 7314 (2012).
12. V. Sridhar, I. Lee, H. H. Chun, and H. Park, *eXPRESS Polym. Lett.*, **7**(4), 320 (2013).
13. W. S. Hummers and R. E. Offeman, *J. Am. Chem. Soc*., **80**, 1339 (1958).
14. O. Akhavan, *Carbon*, **48**, 509 (2010).
15. H. X. Xiang, S. H. Chen, Y. H. Cheng, Z. Zhou, and M. F. Zhu, *eXPRESS Polym. Lett.*, **7**, 778 (2013).
16. P. G. Ren, D. X. Yan, X. Ji, T. Chen. and Z. M. Li, *Nanotechnology*, **22**, 055705 (2011).
17. K. L. Dagnon, H. H. Chen, L. H. Innocentini-Mei, and N. A. D'Souza, *Polym. Comp.*, **58**, 133 (2009).
18. J. Sandler, A. H. Windle, P. Werner, V. Altstädt, M. V. Es, and M. S. P. Shaffer, *J. Mater. Sci.*, **38**, 2135 (2003).
19. M. Lai, J. Li, J. Yang, J. Liu, X. Tong, and H. Cheng, *Polym. Int.*, **53**, 1479 (2004).
20. H. W. Ha, A. Choudhury, T. Kamal, T. H. Kim, and S. Y. Park, *ACS Appl. Mater. Interf.*, **4**, 4623 (2012).
21. S. Mikhailov, *Physics and Applications of Graphene-Experiments*, InTech Janeza Trdine Rijeka, Croatia (2011).